Received February 2002
Revised December 2002
Accepted December 2002

Application of the conservation element and solution element method in numerical modeling of heat conduction with melting and/or freezing

A. Ayasoufi and T.G. Keith
Department of Mechanical, Industrial and Manufacturing Engineering, The University of Toledo, OH, USA

Keywords *Numerical methods, Conduction, Melting*

Abstract *The conservation element and solution element (CE/SE) method, an accurate and efficient explicit numerical method for resolving moving discontinuities in fluid mechanics problems, is used for the first time to solve phase change problems. Several isothermal phase change cases are studied and comparisons are made to existing analytical solutions. The CE/SE method is found to be accurate and robust for the numerical modeling of phase change problems.*

Introduction

Heat flow accompanied by melting and/or solidification occurs in many physical phenomena and has considerable industrial application in a variety of fields. For example, phase change processes are a very efficient means of maintaining a system's temperature within an operating range (Sulfredge *et al.*, 1992); phase change problems occur in the casting of metals; and phase change problems are involved in the formation of ice layers on the oceans as well as on aircraft surfaces. Because of its importance, accurate and robust methods of modeling phase change problems are of great interest.

The characteristic of phase-change problems is that, in addition to the temperature field, the location of the interface is unknown. Problems of this kind arise in fields such as molecular diffusion, friction and lubrication, inviscid flow, etc. (Alexiades and Solomon, 1993). Overviews of such problems, referred to as *moving boundary problems* or *free boundary problems* may be found in Crank (1984), Elliott and Ockendon (1982) and Rubinsteĭn (1971).

There exists two principle approaches for modeling phase change problems: first is the *phase front fitting* in which explicit tracking of the phase change boundary is followed by using moving grid schemes. One example of the methods of this category is the method of Douglas and Gallie (1955) which is

International Journal of Numerical Methods for Heat & Fluid Flow
Vol. 13 No. 4, 2003
pp. 448-472

0961-5539
DOI 10.1108/09615530310475902

based on using a set spatial step while the time step floats. Another example is the isotherm migration method of Crank (1984) which is based on using a set time step with two distinct, and time-varying, space steps for the two phases. Surveys of front tracking methods appear in Crank (1984). The phase front fitting methods, however, often require complicated starting solutions (Boley, 1968), and are inapplicable for materials that change phase over a temperature interval rather than at a single specified temperature. Moreover, these methods are difficult to extend to multidimensional problems.

Secondly, *Phase front capturing* methods which automatically determine the location of the phase front from the formulation of the problem. These methods offer a more suitable approach for modeling a general phase change problem. The most prominent of the phase capture schemes is the *enthalpy method* which is based upon the method of weak solutions (Atthey, 1975; Ockendon, 1975), and, by incorporating the latent heat of fusion in the formulation, provides the location of the liquid/solid interface as an integral part of the solution (Voller and Cross, 1981). Numerical application of these methods, however, produces better results when the phase change occurs within a temperature range. For situations where the phase change occurs at a single temperature, the phase front is a moving discontinuity. Consequently, all of these methods need regularization and special adjustments in order to achieve convergence and stability of the numerical solution (Celentano and Pérez, 1996) and to avoid oscillations in the location of the interface.

The method of space-time conservation element and solution element (CE/SE) was developed by Chang and To (1991) and Chang *et al.* (1999, 2000) at the NASA Glenn Research Center in order to solve the conservation laws. Since its inception 10 years ago, the method has been found capable of accurately resolving shock waves and contact discontinuities without introducing numerical oscillations (Wang *et al.*, 1998). The CE/SE method has been used to obtain highly accurate numerical solutions for solving two-dimensional and axisymmetric inviscid flows (Loh and Zaman, 2002; Loh *et al.* 2001), quasi-one-dimensional inviscid flows (Wang *et al.*, 2000), and two- and three-dimensional viscous flows (Chen and Liu, 2000; Guo *et al.*, 2000). In particular, problems involving shock waves, rarefaction waves, acoustic waves, vortices, ZND detonation waves, shock/acoustic wave/vortex interactions, a dam-break and a hydraulic jump (Molls and Molls, 1998) have been investigated using the method. Yang *et al.* (2001) have also proved a mathematical discussion on the convergence and error bound analysis of the CE/SE method applied to a one-dimensional time-dependent convection-diffusion equation.

It has been shown that the CE/SE method is genuinely robust, i.e. unlike many other shock capturing schemes the accuracy of the CE/SE results is achieved without resorting to special treatment for each individual case (Liu and Chen, 1999).

This new framework for solving conservation laws differs substantially in both concept and methodology from the traditional methods, i.e. finite difference, finite volume, finite element, and spectral methods. Among the above methods, finite difference, finite element, and spectral methods are designed to solve the differential form of the conservation laws. The differential forms are obtained from the integral forms with the assumption that the physical solution is smooth. This assumption becomes a difficulty in the presence of discontinuities. Thus, a method designed to obtain numerical solution to the differential form without enforcing flux conservation has a fundamental disadvantage in modeling discontinuities (Chang, 1995). The CE/SE method is developed on the basis of local and global flux conservation in a space-time domain in which space and time are treated in a unified manner (Chang *et al.*, 1996). This method is designed to enforce flux conservation in space and time, both locally and globally. This feature is the key to the CE/SE method's capability to accurately capture discontinuities. Among the traditional methods, the finite volume method is the only one designed to enforce flux conservation. However, this method requires flux evaluation on the interface of neighboring cells, which is accomplished using interpolation or extrapolation and generally requires an *ad hoc* choice of a special flux model among many existing models. In the CE/SE method, flux conservation is achieved without complexity, since flux evaluation is an integral part of the solution procedure. Advantages of the CE/SE method compared to traditional methods, i.e. finite difference, finite volume, finite element, and spectral methods are discussed in detail in Chang (1995).

The CE/SE method used here is explicit and, therefore, it is computationally efficient. Moreover, it is conceptually simple, easy to implement and readily extendable to higher dimensions. Despite its second-order accuracy, this method possesses low dispersion errors and low dissipation. These distinguishing features of this newly designed method suggest that it would be a good alternative for numerical simulation of isothermal phase change problems. The application of the present method, however, is not limited to isothermal cases. The present scheme can readily be applied to the cases where the change of phase occurs over a temperature range.

In this paper, the problem formulation using the enthalpy method is briefly presented and then the CE/SE method is described for numerical simulation of phase change problems using unstructured meshing which is selected because of its flexibility for handling complex geometries. Several cases are studied to validate the numerical results. The error behavior of the scheme for different time steps and its performance at the limit of small Stefan numbers are also studied numerically.

Governing equation, enthalpy method

The enthalpy method is used for modeling heat conduction with phase change phenomenon. This method gives the solid-liquid interface as a part of the solution without explicit tracking. The governing equation, i.e. the conservation of energy, with the assumption of constant thermophysical properties within each phase is the Fourier-Biot equation that for a two-dimensional Cartesian coordinate system is written as

$$\rho c \frac{\partial T}{\partial t} = \frac{\partial}{\partial x}\left(k \frac{\partial T}{\partial x}\right) + \frac{\partial}{\partial y}\left(k \frac{\partial T}{\partial y}\right) + \dot{q} \tag{1}$$

where c, k, and ρ are specific heat, thermal conductivity and density of the material, respectively, and $\dot{q}$ refers to a distributed heat source (or sink) that may be present in the domain, e.g. an electrical heating element. The left hand side of the above equation is related to the change of enthalpy. The enthalpy may be defined as

$$\bar{h} = \int_0^T c \, \mathrm{d}T + \phi L_\mathrm{f} \tag{2}$$

where L_f is the latent heat of fusion and ϕ equals 1 for liquids and 0 for solids. Using the above definition, equation (1) can be written as

$$\frac{\partial H}{\partial t} = \frac{\partial}{\partial x}\left(k \frac{\partial T}{\partial x}\right) + \frac{\partial}{\partial y}\left(k \frac{\partial T}{\partial y}\right) + \dot{q} \tag{3}$$

where $H = \rho\bar{h}$ is the enthalpy per unit volume. To use the above equation when both solid and liquid phases are involved, procedures are needed for both choosing the thermal conductivity and calculating the temperature field from the enthalpy field. Since c is assumed to be constant within each phase, the enthalpy of the liquid and solid can be calculated from equation (2) as

$$\begin{aligned} H_\mathrm{S} &= \rho_\mathrm{S}\left(\int_0^T c_\mathrm{S} \, \mathrm{d}T\right) = \rho_\mathrm{S} c_\mathrm{S} T \\ H_\mathrm{L} &= \rho_\mathrm{L}\left(\int_0^{T_\mathrm{f}} c_\mathrm{S} \, \mathrm{d}T + \int_{T_\mathrm{f}}^T c_\mathrm{L} \, \mathrm{d}T + L_\mathrm{f}\right) \\ &= \rho_\mathrm{L}(c_\mathrm{S} T_\mathrm{f} + c_\mathrm{L}(T - T_\mathrm{f}) + L_\mathrm{f}) \end{aligned} \tag{4}$$

where subscripts L and S refer to liquid and solid phases, respectively, and T_f is the fusion temperature. Therefore, for a material that changes phase at a single temperature, the temperature field can be calculated using equation (4) as follows

$$T = \begin{cases} \frac{H}{\rho_S c_S} & H \le H_{Sf} \\ T_f & H_{Sf} \le H \le H_{Lf} \\ \frac{(H - H_{Lf})}{\rho_L c_L} + T_f & H \ge H_{Lf} \end{cases} \quad (5)$$

where $H_{Lf} = \rho_L(c_S T_f + L_f)$ and $H_{Sf} = \rho_S c_S T_f$ are enthalpies of the fusion liquid and fusion solid, respectively. These values can also be used in the numerical approach for determining whether each grid element is solid, liquid or undergoing melting/freezing.

Corresponding thermal conductivities are then chosen for that grid element. For elements that are undergoing fusion, an average thermal conductivity is used. This average can be either the arithmetic average of solid and liquid values or a linear interpolation between them based on the value of H, both resulting in good simulations.

Numerical method: CE/SE

Consider the following PDE which can represent a variety of conservation laws depending upon the definition of H and the flux functions F and G

$$\frac{\partial H}{\partial t} + \frac{\partial F}{\partial x} + \frac{\partial G}{\partial y} = 0 \quad (6)$$

As a special case note that, for a problem with no generation, equation (3) can be written in the above form defining for example

$$F = -k\frac{\partial T}{\partial x}, \qquad G = -k\frac{\partial T}{\partial y} \quad (7)$$

Considering (x, y, t) as coordinates of a three-dimensional Euclidean space-time, equation (6) can be written as

$$\vec{\nabla} \cdot \vec{U} = 0, \quad \vec{U} = (F, G, H) \quad (8)$$

A two-dimensional, unstructured, space-time mesh is used here which consists of Delaunay triangulation on the xy-plane that, considering the time axis as the third dimension, makes prisms perpendicular to the xy-plane. The computational molecule of this grid is shown in Figure 1(a), where nodes V_1, V_2, and V_3 determine vertices of a triangular cell j at time level $n - 1/2$, with C as its centroid, while points C_1, C_2, and C_3 denote the centroids of three neighboring cells j_1, j_2, and j_3, respectively. Primed points represent the same spatial nodes after half time-step. For each cell, the integral form of the governing equation (equation (8)) may be applied to the octahedral element that is the union of the three tetragonal prisms: $CV_2C_1V_3V'_3C'V'_2C'_1$,

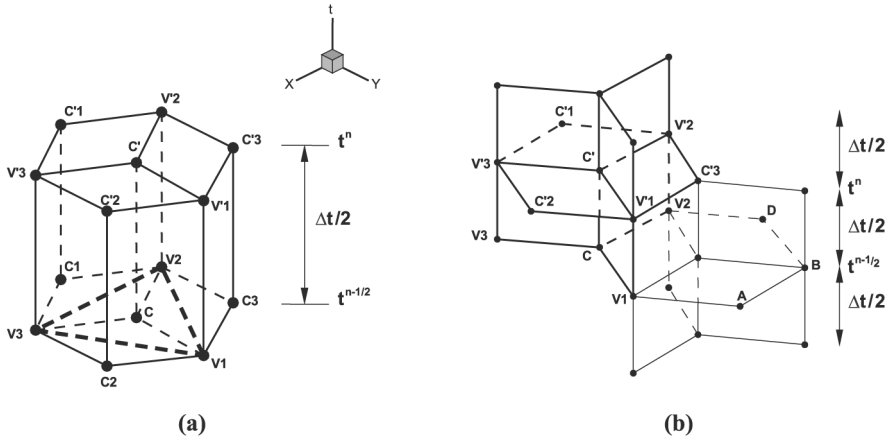

Figure 1.
Computational molecule of CE/SE method, (a) CE's and (b) SE's

$CV_3C_2V_1V_1'C'V_3'C_2'$, and $CV_1C_3V_2V_2'C'V_1'C_3'$. The octahedron will be called the *Conservation Element* of cell j. The integral conservation law will then be

$$\int_{V(\mathrm{CE})} \vec{\nabla}\cdot\vec{U}\,\mathrm{d}V = 0 \tag{9}$$

where V(CE) denotes the volume of the conservation element. Using the divergence theorem, equation (9) implies

$$\int_{S(\mathrm{CE})} \vec{U}\cdot\hat{n}\,\mathrm{d}s = 0 \tag{10}$$

where S(CE) denotes the surface of the conservation element and $\hat{n} = (n_x, n_y, n_t)$ is the unit outward normal to it. In order to perform the above surface integration, $\vec{U}$ may be replaced by a first order Taylor series approximation about a suitably chosen node, (called *a solution point*), where the discretized values of $\vec{U}$ and its derivatives are saved. In this method both $\vec{U}$ and its first-order derivatives are considered as the independent variables which must be determined. By "suitably chosen" it is intended that, solution points may be selected such that the method is explicit, this will be shown later. Let (x_j', y_j') represent the spatial coordinates of the solution point related to cell j. Therefore, components of $\vec{U}$ may be approximated as

$$H(x,y,t;j,n) = H_j^n + (H_x)_j^n(x - x_j') + (H_y)_j^n(y - y_j') + (H_t)_j^n(t - t^n) \tag{11}$$

The same approach may be used for F and G. Further, the derivatives of F and G can be found from equation (7), i.e.

$$F_x = -kT_{xx}, \quad F_y = -kT_{xy}, \quad F_t = -kT_{xt},$$
$$G_x = -kT_{yx}, \quad G_y = -kT_{yy}, \quad G_t = -kT_{yt} \tag{12}$$

where $T_{xx}, T_{xy}, T_{xt}, T_{yx}, T_{yy}$, and T_{yt} are second-order derivatives of temperature and their mesh values will be calculated later in the section of second-order derivatives.

In equation (11), the notation $H(x, y, t; j, n)$ (Wang and Chang, 1999) means the value of H at the point (x, y, t) is evaluated using the entity (j, n). The reason these need to be defined can be explained by considering the fact that each node on any of the surfaces indicated in Figure 1(a) may be evaluated using different discrete values, e.g. the value of $\vec{U}$ at a point on the $CV_1V_1'C'$ plane may be found using the expansion point of cell j at time level n as well as time level $n - 1/2$. Also, the value of $\vec{U}$ at a point on the $CV_2C_1V_3$ plane may be found using the expansion point of cell j at time level $n - 1/2$ as well as that of the neighboring cell, j_1. To assign a unique value to each node while integrating, each surface needs to be related to one and only one (j, n) entity, which is called a *solution element*. Consequently, these entities must be defined as a combination of non-overlapping surfaces that decompose the entire domain. Figure 1(b) shows two of four solution elements related to the cell j, i.e. SE (j, n) which consists of the hexagon $C_1'V_3'C_2'V_1'C_3'V_2'$ combined with three vertical rectangular planes cutting through it, SE $(j_3, n - 1/2)$ that consists of the hexagon CV_1ABDV_2 combined with three vertical rectangular planes cutting through it, where A, B, and D are related to the neighbor j_3 of cell j (not shown), and two other SE's $(j_1, n - 1/2)$ and $(j_2, n - 1/2)$ that are built the same way. Using the notation convention introduced in Zhang *et al.* (2002), consider the SE $(j_1, n - 1/2)$. The area of two lateral faces related to this SE, i.e. $C_1V_2V_2'C_1'$ and $C_1V_3V_3'C_1'$ (see Figure 1(a)) will be referred to as $S^{(1,1)}$, and $S^{(2,1)}$, respectively, while $\hat{n}^{(1,1)}$, and $\hat{n}^{(2,1)}$ represent the unit normals of the above lateral faces, outward with respect to the octahedron. Furthermore, spatial coordinates of the centroid of each of these faces will be referred to as $(x_c^{(1,1)}, y_c^{(1,1)})$, and $(x_c^{(2,1)}, y_c^{(2,1)})$, respectively. Also the area of $C_1V_3CV_2$, that is the horizontal plane related to this SE, will be called $S^{(1)}$ while $(0, 0, -1)$ represents its unit outward normal.

In general, for SE $(j_k, n - 1/2)$, $k = 1, 2, 3$, area, unit outward normal, and the spatial coordinates of the centroid of the lateral faces will be referred to as $S^{(l,k)}$, $\hat{n}^{(l,k)} = (n_x^{(l,k)}, n_y^{(l,k)}, 0)$, and $(x_c^{(l,k)}, y_c^{(l,k)})$, $l = 1, 2$. Also the area, and the spatial coordinates of the centroid of the corresponding horizontal plane will be represented by $S^{(k)}$, and $(x_c^{(l,k)}, y_c^{(l,k)})$, respectively. Note that the so-called horizontal planes form the bottom of the octahedron. The horizontal planes that contain the top of the octahedron, however, belong to SE (j, n). The area and spatial coordinates of the centroid of the top surfaces are equal to those of the bottom surfaces but their unit outward normal is $(0, 0, +1)$. Using the above conventions and performing the inner products, equation (10) can be written as

$$\int_{S(\mathrm{CE})} \vec{U}\cdot\hat{n}\,\mathrm{d}s = \sum_{k=1}^{3}\left\{\int_{S^{(k)}} H(x,y,t;j,n)(+1)\,\mathrm{d}s + \int_{S^{(k)}} H(x,y,t;j_k,n-1/2)(-1)\,\mathrm{d}s + \sum_{l=1}^{2}\int_{S^{(l,k)}}\left[F(x,y,t;j_k,n-1/2)n_x^{(l,k)} + G(x,y,t;j_k,n-1/2)n_y^{(l,k)}\right]\mathrm{d}s\right\} \tag{13}$$

where the first and second integrals are performed over the top and bottom surfaces, respectively, and the third integral is related to the lateral faces of the octahedral CE.

Using equation (11), the third integral of equation (13) can be evaluated as follows

$$\begin{aligned} I^{(l,k)} &= \int_{S^{(l,k)}}\left[F(x,y,t;j_k,n-{}^1\!/_2)n_x^{(l,k)} + G(x,y,t;j_k,n-{}^1\!/_2)n_y^{(l,k)}\right]\mathrm{d}s \\ &= \int_{S^{(l,k)}}\Big\{\left[F_{j_k}^{n-1/2} + (F_x)_{j_k}^{n-1/2}(x-x'_{j_k})\right. \\ &\quad \left. + (F_y)_{j_k}^{n-1/2}(y-y'_{j_k}) + (F_t)_{j_k}^{n-1/2}(t-t^{n-1/2})\right] n_x^{(l,k)} \\ &\quad + \left[G_{j_k}^{n-1/2} + (G_x)_{j_k}^{n-1/2}(x-x'_{j_k}) + (G_y)_{j_k}^{n-1/2}(y-y'_{j_k})\right. \\ &\quad \left. +(G_t)_{j_k}^{n-1/2}(t-t^{n-1/2})\right] n_y^{(l,k)}\Big\}\,\mathrm{d}s \end{aligned}$$

Rearranging leads to

$$\begin{aligned} I^{(l,k)} &= \int_{S^{(l,k)}}\mathrm{d}s\left\{\left[F_{j_k}^{n-1/2} - (F_x)_{j_k}^{n-1/2}x'_{j_k} - (F_y)_{j_k}^{n-1/2}y'_{j_k} - (F_t)_{j_k}^{n-1/2}t^{n-1/2}\right]n_x^{(l,k)}\right. \\ &\quad \left. +\left[G_{j_k}^{n-1/2} - (G_x)_{j_k}^{n-1/2}x'_{j_k} - (G_y)_{j_k}^{n-1/2}y'_{j_k} - (G_t)_{j_k}^{n-1/2}t^{n-1/2}\right]n_y^{(l,k)}\right\} \\ &\quad + \left[(F_x)_{j_k}^{n-1/2}n_x^{(l,k)} + (G_x)_{j_k}^{n-1/2}n_y^{(l,k)}\right]\int_{S^{(l,k)}} x\,\mathrm{d}s + \left[(F_y)_{j_k}^{n-1/2}n_x^{(l,k)}\right. \\ &\quad \left. + (G_y)_{j_k}^{n-1/2}n_y^{(l,k)}\right]\int_{S^{(l,k)}} y\,\mathrm{d}s + \quad \left[(F_t)_{j_k}^{n-1/2}n_x^{(l,k)} + (G_t)_{j_k}^{n-1/2}n_y^{(l,k)}\right]\int_{S^{(l,k)}} t\,\mathrm{d}s \end{aligned}$$

But $\int_{S^{(l,k)}}\mathrm{d}s$ is the area of the corresponding lateral face and the rest of the above integrals may be evaluated using the space-time coordinates of its centroid. Therefore, the integral becomes

$$I^{(l,k)} = S^{(l,k)}\left\{\left[F_{j_k}^{n-1/2} + (F_x)_{j_k}^{n-1/2}(x_c^{(l,k)} - x'_{j_k}) + (F_y)_{j_k}^{n-1/2}(y_c^{(l,k)} - y'_{j_k}) + \frac{\Delta t}{4}(F_t)_{j_k}^{n-1/2}\right] n_x^{(l,k)} + \left[G_{j_k}^{n-1/2} + (G_x)_{j_k}^{n-1/2}(x_c^{(l,k)} - x'_{j_k}) + (G_y)_{j_k}^{n-1/2}(y_c^{(l,k)} - y'_{j_k}) + \frac{\Delta t}{4}(G_t)_{j_k}^{n-1/2}\right] n_y^{(l,k)}\right\}$$

Based on equation (11), $I^{(l,k)}$ can also be written as

$$I^{(l,k)} = \{F(x_c^{(l,k)}, y_c^{(l,k)}, t^n - \Delta t/4;\ j_k, n - {}^1/_2) n_x^{(l,k)} + G(x_c^{(l,k)}, y_c^{(l,k)}, t^n - \Delta t/4;\ j_k, n - {}^1/_2) n_y^{(l,k)}\} S^{(l,k)} \tag{14}$$

Following a similar procedure, the first and second integrals of equation (13) become

$$\int_{S^{(k)}} H(x,y,t;\ j,n)(+1)\,\mathrm{d}s = S^{(k)}\left[H_j^n + (H_x)_j^n(x_c^{(k)} - x'_j) + (H_y)_j^n(y_c^{(k)} - y'_j)\right] \tag{15}$$

and

$$\int_{S^{(k)}} H(x,y,t;\ j_k, n-1/2)(-1)\,\mathrm{d}s = -S^{(k)}\left[H_{j_k}^{n-1/2} + (H_x)_{j_k}^{n-1/2}(x_c^{(k)} - x'_{j_k}) + (H_y)_{j_k}^{n-1/2}(y_c^{(k)} - y'_{j_k})\right] = -S^{(k)} H(x_c^{(k)}, y_c^{(k)}, t^{n-1/2};\ j_k, n-1/2) \tag{16}$$

respectively.

Equation (13), after substitution of the evaluated integrals, provides an expression for H_j^n. The expression contains three unknowns $H_j^n, (H_x)_j^n$, and $(H_y)_j^n$, but examination of the expressions which contain $(H_x)_j^n$ and $(H_y)_j^n$ suggests that they may be eliminated, resulting in an explicit method, provided the solution point is selected at the centroid of the hexagon $C_1V_3C_2V_1C_3V_2$ formed by the vertices of cell j and the centroids of its three neighbors. Using this, the equation for H_j^n can be written in a convenient manner. Note that despite the apparent complexity, the equation for H_j^n is in fact composed of three similar parts, each related to one of the neighboring cells.

$$H_j^n = \frac{\sum_{k=1}^{3} R^{(k)}}{\sum_{k=1}^{3} S^{(k)}} \tag{17}$$

where

$$R^{(k)} = S^{(k)} H(x_c^{(k)}, y_c^{(k)}, t^{n-1/2}; j_k, n-1/2) - \sum_{l=1}^{2} I^{(l,k)}$$

and $I^{(l,k)}$ is evaluated using equation (14).

The above formulation has the important attribute of being able to handle non-linearities that may exist in the definition of functions H, F and G.

Once the values of enthalpy are updated over the entire domain, equation (5) can be used to obtain the temperature field, and the first and second order derivatives of the field parameters may be calculated as described in the following sections.

First order derivatives

Consider Figure 2, where S, S_1, S_2, and S_3 are solution points of cell j and its three neighbors, respectively, also O_1, O_2, and O_3 denote centroids of triangles SS_2S_3, SS_3S_1, and SS_1S_2, respectively. Using Taylor series in triangle SS_2S_3, as described in Liu and Chen (2001), the following equations can be written

$$H_{O_1} + (x'_j - x_{O_1})(H_x)^n_{O_1} + (y'_j - y_{O_1})(H_y)^n_{O_1} = H^n_j$$

$$H_{O_1} + (x'_{j_2} - x_{O_1})(H_x)^n_{O_1} + (y'_{j_2} - y_{O_1})(H_y)^n_{O_1} = H^n_{j_2}$$

$$H_{O_1} + (x'_{j_3} - x_{O_1})(H_x)^n_{O_1} + (y'_{j_3} - y_{O_1})(H_y)^n_{O_1} = H^n_{j_3}$$

which, after some algebraic manipulations, imply the following two equations

$$(x'_{j_k} - x'_j)(H_x)^n_{O_1} + (y'_{j_k} - y'_j)(H_y)^n_{O_1} = H^n_{j_k} - H^n_j$$

where $k = 2, 3$. The above system can be solved to give $(H_x)^n_{O_1}$ and $(H_y)^n_{O_1}$. A similar procedure can be used in triangles SS_3S_1, and SS_1S_2 to obtain two other systems

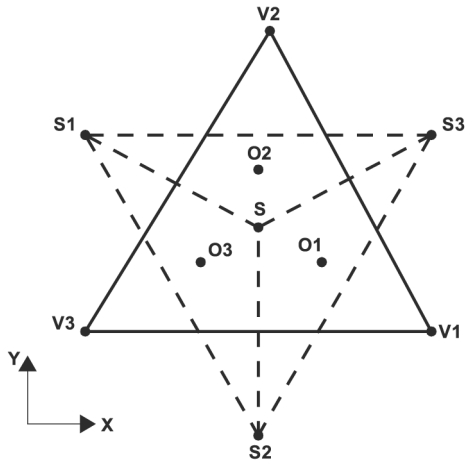

Figure 2.
Geometry for calculating 1st-order derivatives

$$(x'_{j_k} - x'_j)(H_x)^n_{O_2} + (y'_{j_k} - y'_j)(H_y)^n_{O_2} = H^n_{j_k} - H^n_j$$

with $k = 1, 3$, and

$$(x'_{j_k} - x'_j)(H_x)^n_{O_3} + (y'_{j_k} - y'_j)(H_y)^n_{O_3} = H^n_{j_k} - H^n_j$$

with $k = 1, 2$. These systems can be solved to determine the derivatives at O_2 and O_3. A weighted average may then be used to calculate $(H_x)^n_j$ and $(H_y)^n_j$ as follows

$$(H_x)^n_j = \frac{\sum_{k=1}^{3} |\theta_m \theta_p|^{\tilde{\alpha}} (H_x)^n_{O_k}}{\sum_{k=1}^{3} |\theta_m \theta_p|^{\tilde{\alpha}}}, \quad (H_y)^n_j = \frac{\sum_{k=1}^{3} |\theta_m \theta_p|^{\tilde{\alpha}} (H_y)^n_{O_k}}{\sum_{k=1}^{3} |\theta_m \theta_p|^{\tilde{\alpha}}} \tag{18}$$

where

$$\theta_k = \sqrt{[(H_x)^n_{O_k}]^2 + [(H_y)^n_{O_k}]^2}, \quad k = 1, 2, 3$$

and *kmp* is a non-neutral permutation of 1, 2, 3, and the constant $\tilde{\alpha}$ is usually set equal to 1. The above weighted average provides the necessary numerical damping (Liu and Chen, 2001). Note that, to avoid dividing by zero, in practice a small positive number such as 10^{-60} is added to the denominators in equation (18). The same technique can be used to calculate the first-order derivatives of temperature.

One can also obtain the same values for the first-order derivatives, without introducing points O_1, O_2, and O_3. The reader is referred to Wang and Chang (1999) for details.

Second order derivatives

Consider Figure 2, as explained in Liu and Chen (2001), once the first order derivatives of a field parameter (say Ψ) are known, expanding $(\Psi_x)^{n-1/2}_{j_k}, k = 1, 2, 3$, which is saved at the solution point $(S_k, n - 1/2)$ about the space-time solution point (S, n), results in three equations

$$(x'_{j_k} - x'_j)(\Psi_{xx})^n_j + (y'_{j_k} - y'_j)(\Psi_{xy})^n_j - \frac{\Delta t}{2}(\Psi_{xt})^n_j = (\Psi_x)^{n-1/2}_{j_k} - (\Psi_x)^n_j, \quad k = 1, 2, 3$$

These may be solved simultaneously for $(\Psi_{xx})^n_j$, $(\Psi_{xy})^n_j$, and $(\Psi_{xt})^n_j$. A similar system gives $(\Psi_{yx})^n_j$, $(\Psi_{yy})^n_j$, and $(\Psi_{yt})^n_j$. Using this technique, the mesh values of second-order derivatives of T can be evaluated in order to be used in equation (12). The first-order derivatives of flux functions, evaluated from equation (12), can then be used in equation (17).

Boundary conditions

In order to treat the boundary conditions, a ghost cell is defined for each boundary cell. Geometrically, the ghost cell is a mirror image of the corresponding boundary cell with respect to the boundary, as shown in Figure 3 where S_j and S_g denote solution points related to the boundary cell and the ghost cell, respectively, and B is the intersection of the line S_g and S_j with the boundary.

Let Ψ be a field parameter, which can be either enthalpy or temperature.

(1) Constant temperature boundary $\Psi_B = \text{Const}$:

Using a linear interpolation

$$\Psi_g = 2\Psi_B - \Psi_j$$

All the derivatives at "g" may then be set equal to their corresponding values at "j".

(2) Reflecting boundary condition; the insulated boundary, axis of symmetry:

Let σ and τ be the normal and tangential directions to the boundary, respectively. The insulation condition is then

$$\left(\frac{\partial T}{\partial \sigma}\right)_{\text{boundary}} = 0$$

and considering

$$\frac{\partial H}{\partial \sigma} = c\,\frac{\partial T}{\partial \sigma}$$

it also leads to

$$\left(\frac{\partial H}{\partial \sigma}\right)_{\text{boundary}} = 0.$$

The reader is referred to Wang and Chang (1999) for details of reflecting boundary conditions.

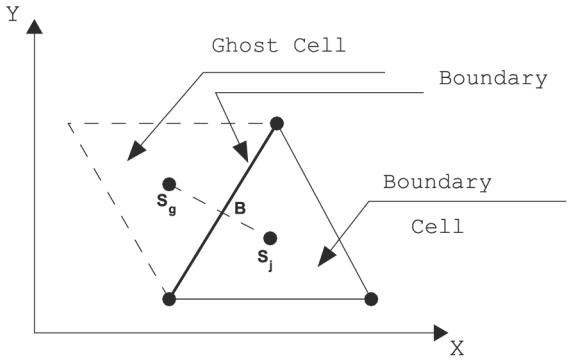

Figure 3.
Boundary and ghost cells

Results and discussion

To assess the accuracy and effectiveness of the CE/SE method applied to conduction problems with phase change, several classical cases were solved and the results were compared to the analytical solutions.

In order to validate the computer program and study the error behavior of the numerical scheme, the following two cases were designed and applied to a unit square geometry, with $k = 1$.

$$\text{Case 1. } H = T \text{ and } T = x + y, \tag{19}$$

$$\text{Case 2. } H = T \text{ and } T = 2t + (x^2 + y^2)/2. \tag{20}$$

As can be seen, the above temperature distributions satisfy the governing equation (equation (3)).

Case 1

This case is a steady first-order problem, for which it can be easily shown that the CE/SE formulation is exact, in the sense that no truncation error exists. Therefore, the spatial grid is not an issue in this case. On the other hand, the time-step issue needs to be studied. Equation (19) was applied on the boundaries, with an initially imposed error distribution over the entire domain. The results confirmed that, after a period of time, the temperature converges to the accurate distribution everywhere in the field.

Time-step considerations and error behavior. The error behavior was studied, for the steady case above, for different time-steps. Since the present method is explicit, there are stability restrictions on the time-step. Usage of a time-step larger than the spatial grid size, leads to divergence. By reducing the time-step, it was found that the numerical errors grow, but there is an upper bound for this growth. This can be seen in Figure 4, where absolute error (norm of infinity of the difference between the numerical and exact solutions) is depicted versus the iterations. This region where errors grow will be referred to as region A. Further reduction of the time-step results in stable accurate solutions. Although there is a very small lower bound to the vanishing errors, the results of this region can be considered independent of time-step. This is shown in Figure 5. As can be seen, the fastest convergence rate is achieved by using the largest time-step that falls in this category. This region will be referred to as region B. Figure 5 also shows that once the lower bound is achieved, the errors do not start to grow with further iteration. Additional numerical experiments confirmed the following facts:

(1) the same pattern was detected for other problems,

(2) once the time-step is selected for a spatial mesh, it can be used for other phase-change problems on the same mesh.

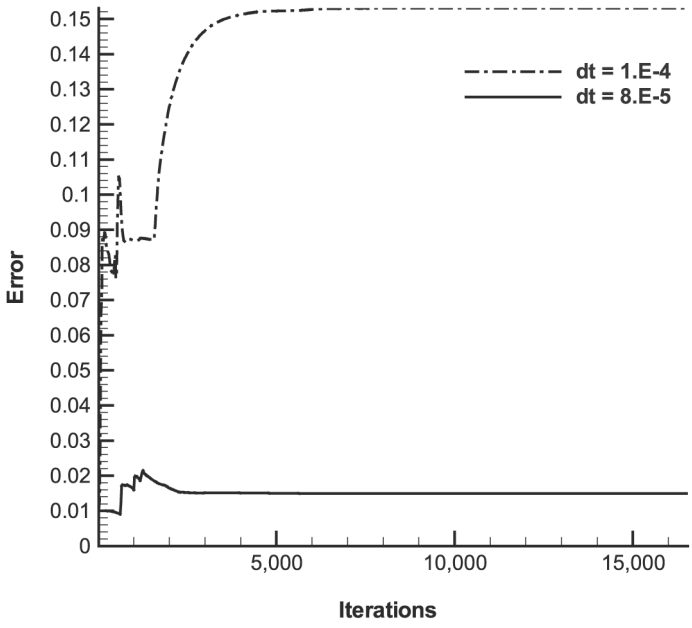

Figure 4.
Bounded growth of errors (region *A*)

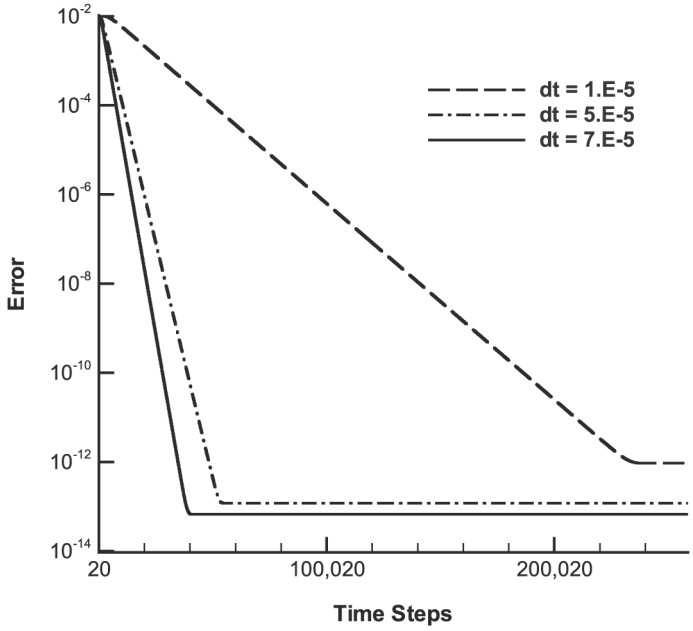

Figure 5.
Vanishing errors (region *B*)

It is worthwhile to note that in both regions, A and B, a stable converged solution is achievable, while only one of them gives the correct solution. This problem can be easily resolved noting that by slightly changing the time-step in region A, results change dramatically, a phenomenon that does not occur in region B. Based on the above results, the procedure of choosing the right time-step for a spatial grid, may be summarized as starting from a large time-step and reducing it until stable, time-step independent results are achieved.

Case 2

For this transient problem, unlike the previous case, there is a truncation error associated with second-order accuracy of the CE/SE method. Clearly, this error should decrease by using finer spatial grids. Two spatial grids were used for this case. A grid that has 50 nodes on each side of the unit square will be referred to as the coarse grid, while the so-called fine grid consists of 100 nodes on each side of the unit square. Equation (20) was applied on the boundaries. Both exact solution and a uniform error distribution were used as initial conditions. The absolute errors (norm of infinity of the difference between the numerical and exact solutions) are shown in Figure 6 and confirm the second-order accuracy of the scheme.

Case 3: freezing of a finite slab

Consider a slab of thickness L with the initial state assumed to be liquid at the fusion temperature T_f (Figure 7). At $t = 0$, the temperature of the surface at

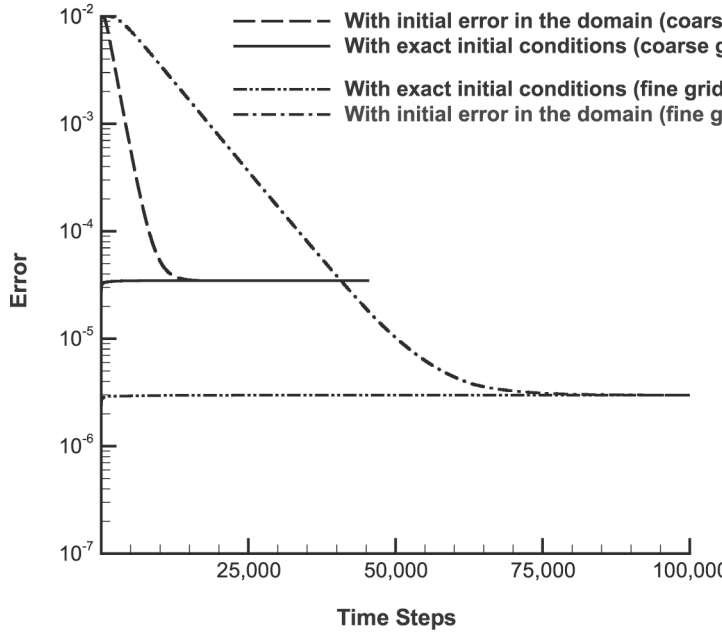

Figure 6.
The grid-dependent truncation error

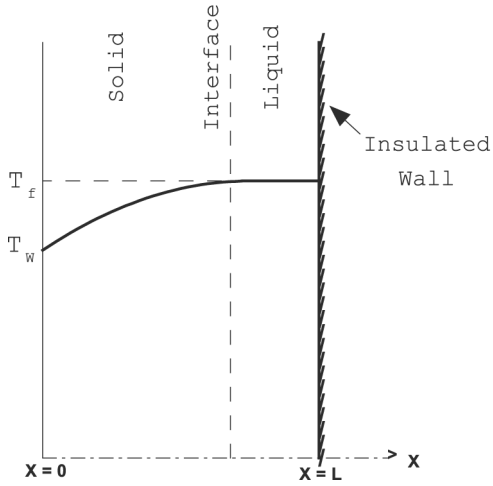

Figure 7.
Geometry of case 3

$x = 0$ drops to T_W and is held there. The surface at $x = L$ is effectively insulated. The analytical solution of this problem, from Lunardini (1981) determines the phase change interface to be at

$$x_{int} = 2\gamma\sqrt{\alpha_s t}$$

where α_s is the thermal diffusivity of the solid phase and γ is defined from solving

$$\gamma e^{\gamma^2} \mathrm{erf}(\gamma) = \frac{c_s(T_f - T_W)}{L_f\sqrt{\pi}}$$

where c_s denotes the specific heat of the solid phase and L_f is the latent heat of fusion.

Also the temperature in the solid region is determined from

$$T = T_W + \frac{T_f - T_W}{\mathrm{erf}(\gamma)}\mathrm{erf}(\eta)$$

where

$$\eta = \frac{x}{2\sqrt{\alpha_s t}}.$$

In order to model this one-dimensional problem using the two-dimensional code, the top and bottom of the slab are assumed to be insulated since any horizontal line can be regarded as a line of symmetry in this problem.

The above problem is studied for a range of different Stefan numbers. Other parameters are $T_W = -1.0$°C, $T_f = 0.0$°C, while the thermal diffusivity

and specific heats are set equal to unity. Figure 8 shows the position of phase-change interface compared to the analytical solution for $S_T = 0.05$, 0.1, 4.0, and 10.0, where $S_T = c_s(T_f - T_W)/L_f$ is the Stefan number. Temperature distributions at $t = 0.14$ s are also compared to the analytical solution in Figure 9. As can be seen, accurate results are obtained for a range of large and small Stefan numbers.

For small Stefan numbers, the accuracy was improved by using a slightly different method for calculation of first-order derivatives. The CE/SE method, in its present form, loses its second-order accuracy and becomes dissipative for $S_T < 1$. The dissipation, however, is adjustable by changing the parameter $\tilde{\alpha}$, as mentioned in the section of first-order derivatives. The accurate results for $S_T = 0.05$,and 0.1 are obtained using $\tilde{\alpha} < 1$. It is possible, however, to design a CE/SE scheme in a way that the above adjustments occur automatically and the method becomes insensitive to the size of Stefan number. An example of such methods is the one-dimensional scheme of Chang (2002).

Case 4: heat conduction with freezing in a corner

The problem under consideration here is the initially liquid infinite corner (Figure 10) at a temperature $T_L \geq T_f$, for time $t \geq 0$ the surfaces $x = 0$ and $y = 0$ are maintained at a constant temperature $T_W < T_f$.

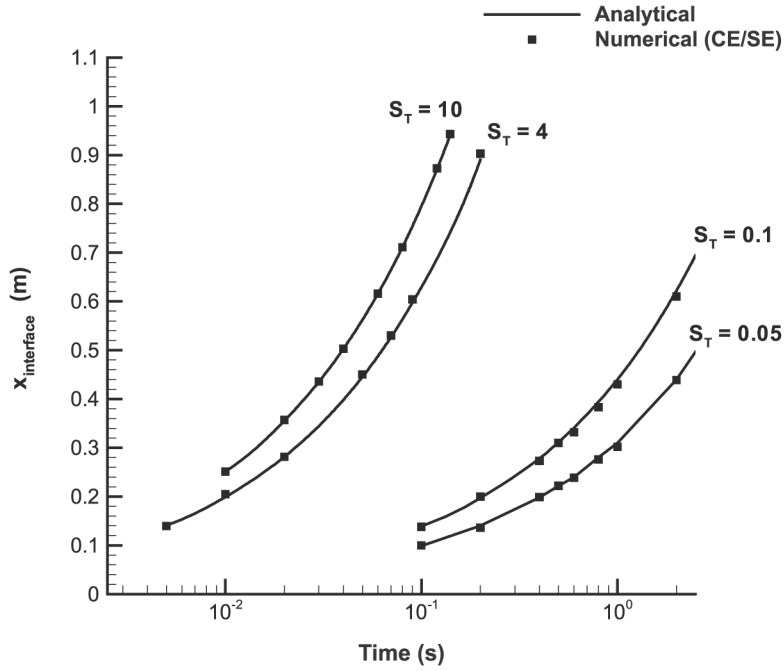

Figure 8.
Location of the interface for case 3

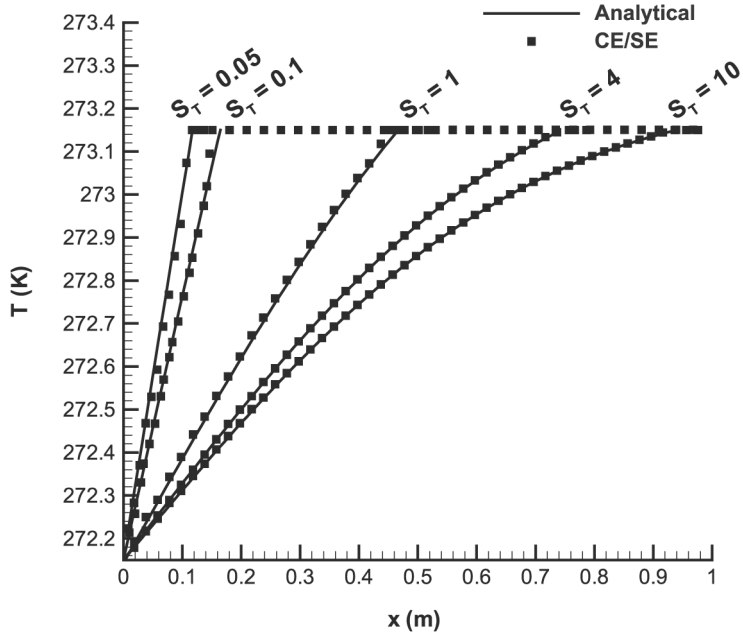

Figure 9.
Temperature distribution at $t = 0.14$ for case 3

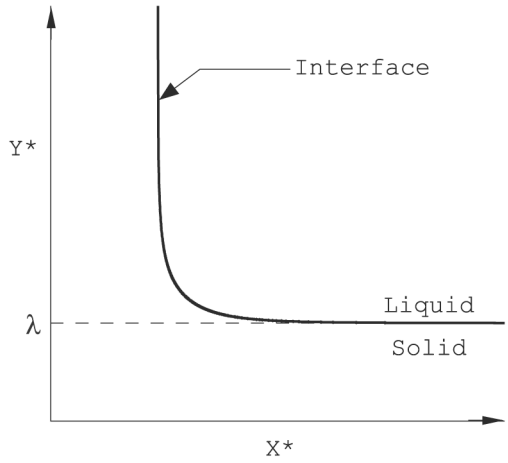

Figure 10.
Geometry for case 4

The analytical solution of this problem is discussed in Rathjen and Jiji (1971). The non-dimensional interface position, $f(x^*)$, can be determined from

$$f(x^*) = \left[\lambda^m + \frac{C}{x^{*m} - \lambda^m}\right]^{\frac{1}{m}} \tag{21}$$

where

$$x^* = \frac{x}{\sqrt{4\alpha t}},$$

α is the thermal diffusivity which is assumed to be equal for both solid and liquid phases, λ (asymptote shown in Figure 10) is calculated solving the following equation

$$\frac{\exp(-\lambda^2)}{\mathrm{erf}(\lambda)} - \frac{T_i^* \exp(-\lambda^2)}{\mathrm{erfc}(\lambda)} = \sqrt{\pi}\beta\lambda$$

where

$$T_i^* = \frac{k_\mathrm{L}}{k_\mathrm{S}}\left(\frac{T_\mathrm{L} - T_\mathrm{f}}{T_\mathrm{f} - T_\mathrm{W}}\right),$$

the non-dimensional initial temperature and

$$\beta = \frac{L_\mathrm{f}}{c_\mathrm{S}(T_\mathrm{f} - T_\mathrm{W})},$$

the latent to sensible heat ratio are two non-dimensional parameters that define this problem. Constants C and m in equation (21) are determined for each case using T_i^* and β (Rathjen and Jiji, 1971). The numerical simulation is performed using insulated walls at $x = 3.0$ and $y = 3.0$. Results are shown for $\beta = 0.25$ and $T_i^* = 0.3$ (which imply $C = 0.159$ and $m = 5.02$ (Ouyang and Tamma, 1996)).

The constant temperature contours, at $t = 0.02\,\mathrm{s}$, are shown in Figure 11 and the non-dimensional interface position is compared to the analytical results in Figure 12. An example of the unstructured mesh for the square cases is shown in Figure 13.

Case 5: inward freezing in a circular pipe

The inward phase change in a cylindrical container is important in dealing with freezing of water in pipes and allied problems, a number of approximate solutions are available for this finite domain problem (Lunardini, 1981). As a result of symmetry, only a quarter of a circle need be studied; the geometry is given in Figure 14 and an example of the spatial mesh is shown in Figure 15. The numerical results are obtained for a quarter circle of unit radius with the initial state assumed to be liquid at the fusion temperature. Other parameters are $T_\mathrm{W} = -1.0$°C, $T_\mathrm{f} = 0.0$°C, and $L_\mathrm{f} = 0.25\,\mathrm{J/kg}$ while the thermal diffusivity and specific heats are set equal to unity. The position of the phase change interface at different times is shown in Figure 16, these graphs are generated using enthalpy contours that range from H_Sf to H_Lf. The enthalpy distribution in the circle is given in Figure 17 for an intermediate time of

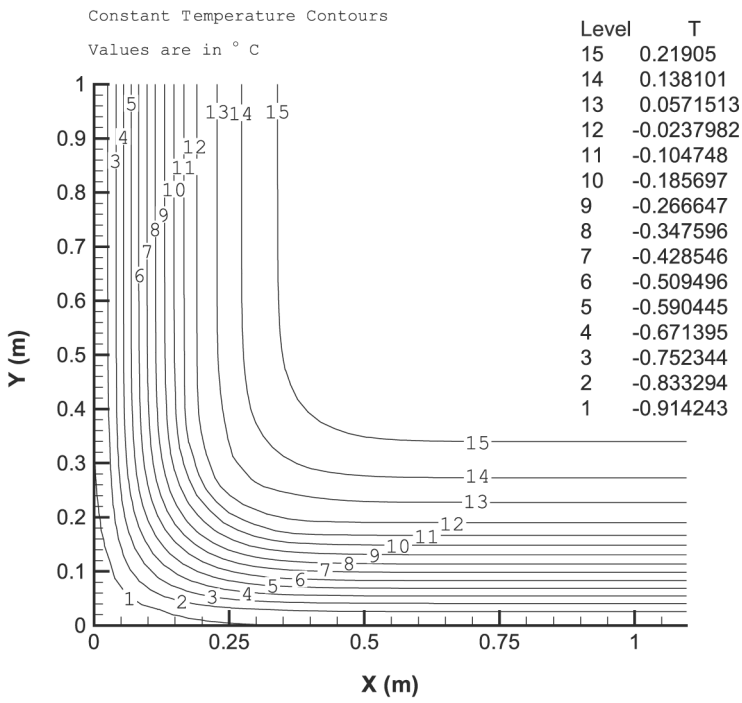

Figure 11.
Temperature isotherms at $t = 0.02$ s

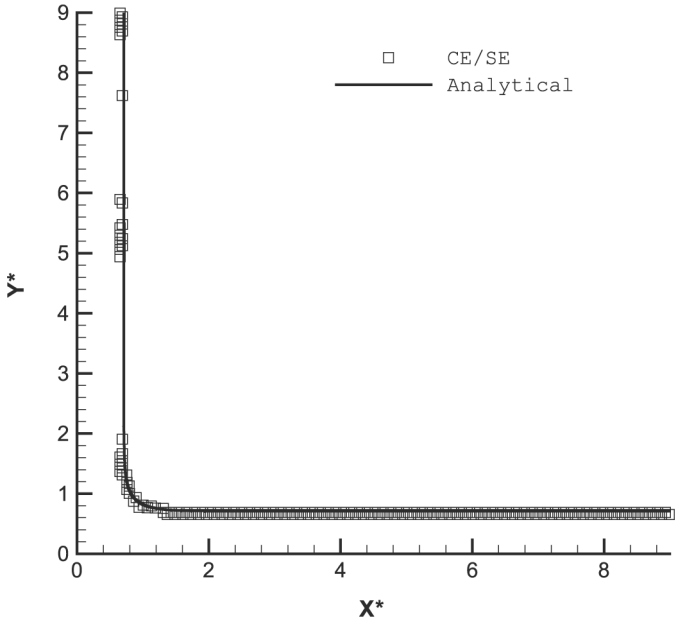

Figure 12.
Non-dimensional interface for case 4

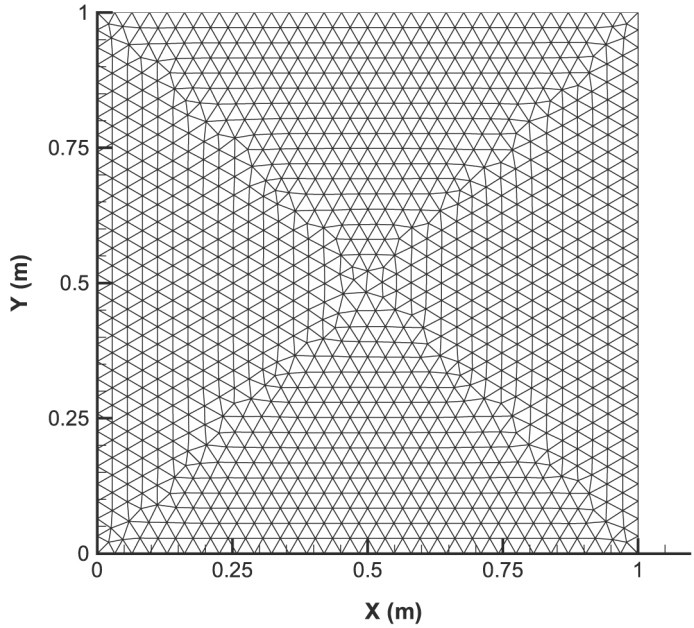

Figure 13.
An example of the square grid

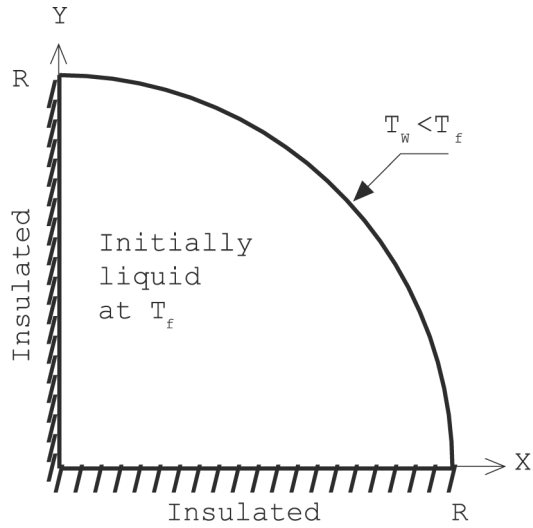

Figure 14.
Geometry of case 5

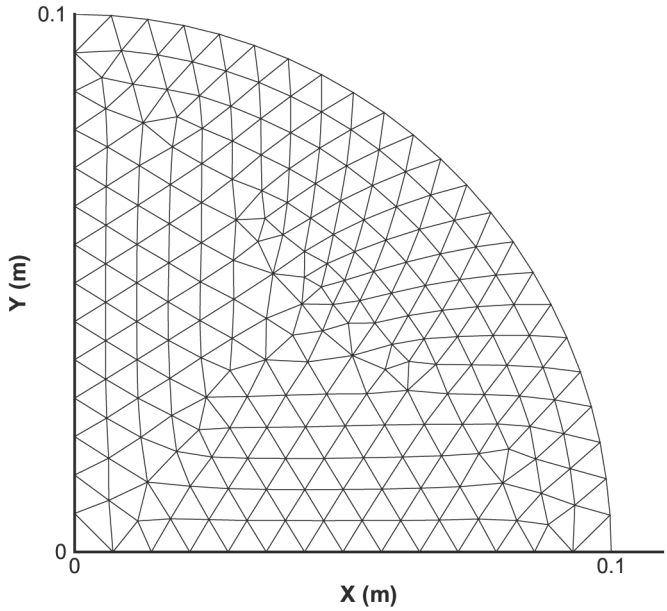

Figure 15.
An example mesh for case 5

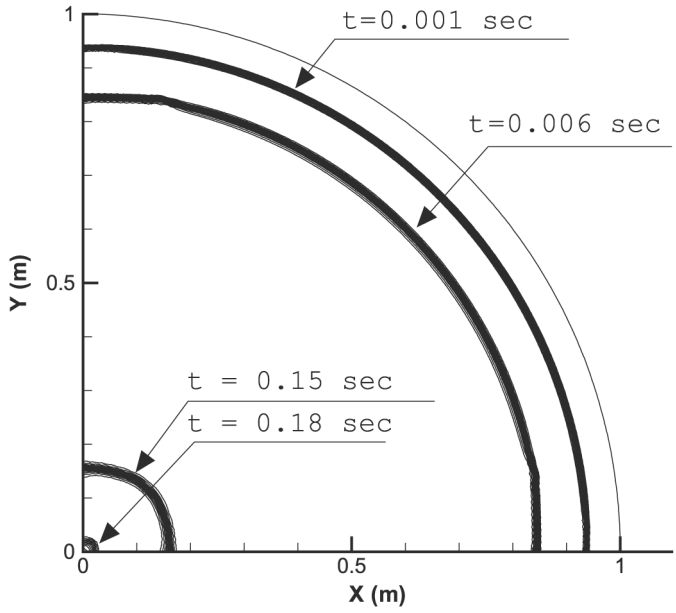

Figure 16.
The interface position for case 5

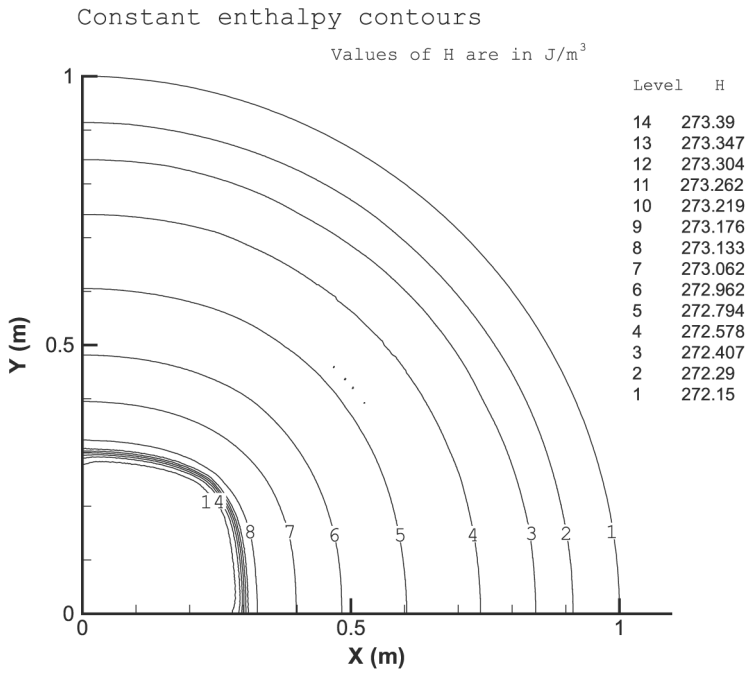

Figure 17.
Enthalpy contours at $t = 0.11$ s

$t = 0.11$ s. The total freezing time (t_f) is determined to be between 0.18 and 0.19 s, which is in agreement with the approximate solution given in Lunardini (1981). This approximate solution may be expressed as

$$\frac{\alpha t_f}{R^2} = \frac{1}{4S_T} + \frac{1}{8}$$

where R is the radius of the circle, α denotes the diffusivity, and the Stefan number S_T can be calculated from

$$S_T = \frac{c_S(T_f - T_W)}{L_f}$$

This approximate relation, for this case, gives a total freezing time of $t_f = 0.1875$ s.

Conclusions

The CE/SE method has been shown to be an accurate and efficient method for resolving discontinuities in fluid mechanics problems. This method was used as a new alternative for solving phase change problems. Comparison of the results to analytical and semi-analytical existing solutions verifies the ability of the method to capture moving phase fronts without incurring oscillations.

The CE/SE method is computationally efficient since it is explicit and requires no iterations to achieve convergence within the same time-step. Moreover, it is conceptually simple, easy to implement and genuinely multi-dimensional. Despite its second-order accuracy, this method possesses low dispersion errors and low dissipation, except for the limit of small Stefan numbers where the method becomes dissipative. The dissipation, however, is adjustable and was shown that accurate results can be obtained for the limit of small Stefan numbers. Several cases were studied and the accuracy of the CE/SE method was verified for this application.

References

Alexiades, V. and Solomon, A.D. (1993), *Mathematical Modeling of Melting and Freezing Processes*, Hemisphere, Washington DC, USA.

Atthey, D.R. (1975), "A finite difference scheme for melting problems based on the method of weak solutions", in Ockendon, J.R. and Hodgkins, W.R. (Eds), *Moving Boundary Problems in Heat Flow and Diffusion*, Clarendon Press, Oxford, p. 182.

Boley, B.A. (1968), "A general starting solution for melting and solidifying slabs", *Int. J. Eng. Sci.*, Vol. 6, p. 89.

Celentano, D. and Pérez, E. (1996), "A phase-change temperature-based formulation including general latent heat effects", *Int. J. Numer. Methods for Heat and Fluid Flow*, Vol. 6 No. 8, pp. 71-9.

Chang, S.C. (1995), "The method of space-time conservation element and solution element – a new approach for solving the Navier-Stokes and Euler equations", *Journal of Computational Physics*, Vol. 119, pp. 295-324.

Chang, S.C. (2002), "Courant number insensitive CE/SE schemes", AIAA 2002-3890.

Chang, S.C. and To, W.M. (1991), "A new numerical framework for solving conservation laws – the method of space-time conservation element and solution element", NASA TM 104495.

Chang, S.C., Wang, X.Y. and Chow, C.Y. (1999), "The space-time conservation element and solution element method: a new high resolution and genuinely multidimensional paradigm for solving conservation laws", *Journal of Computational Physics*, Vol. 156, pp. 89-136.

Chang, S.C., Wang, X.Y. and To, W.M. (2000), "Application of the space-time conservation element and solution element method to one-dimensional convection-diffusion problems", *Journal of Computational Physics*, Vol. 165, pp. 189-215.

Chang, S.C., Yu, S.T., Himansu, A., Wang, X.Y., Chow, C.Y. and Loh, C.Y. (1996), "The method of space-time conservation element and solution element – a new paradigm for numerical solution of conservation laws", *Computational Fluid Dynamics Review*, UK.

Chen, K.H. and Liu, N.S. (2000), "Navier-Stokes solution of the FLUX code: a module for the NCC solver using the concept of space-time conservation element and solution element", AIAA 2000-0455.

Crank, J. (1984), *Free and Moving Boundary Problems*, Clarendon Press, Oxford.

Douglas, J. and Gallie, T. (1955), "On the numerical integration of a parabolic differential equation subject to a moving boundary condition", *Duke Math. J.*, Vol. 22, pp. 557-71.

Elliott, C.M. and Ockendon, J.R. (1982), "Weak and variational methods for moving boundary problems", *Pitman Advanced Publishing Program.*

Guo, Y., Hsu, A.T., Wu, J., Yang, Z. and Oyedrian, A. (2000), "Extension of CE/SE method to 2D viscous flows", *36th AIAA/ASME/SAE/ASEE Joint Propulsion Conference and Exhibit*, 17-19 July 2000.

Liu, N.S. and Chen, K.H. (1999), "FLUX: an alternative flow solver for the national combustion code", AIAA 99-1079.

Liu, N.S. and Chen, K.H. (2001), "An alternative flow solver for the NCC – the FLUX code and its algorithm", *39th AIAA Aerospace Sciences Meeting and Exhibit*, Reno, NV.

Loh, C.Y. and Zaman, K.B.M.Q. (2002), "Numerical investigation of 'Transonic resonance' with a convergent-divergent nozzle", *AIAA Journal*, Vol. 40 No. 12, pp. 2393-401.

Loh, C.Y., Hultgren, L.S. and Chang, S.C. (2001), "Wave computation in incompressible flow using the space-time conservation element and solution element method", *AIAA Journal*, Vol. 39 No. 5, pp. 794-801.

Lunardini, V.J. (1981), *Heat Transfer in Cold Climates*, Van Nostrand Reinhold, NY.

Molls, T. and Molls, F. (1998), "Space-time conservation method applied to Saint Venant equations", *Journal of Hydraulic Engineering*, Vol. 125 No. 5, pp. 501-8.

Ockendon, J.R. (1975), "Techniques of analysis", in Ockendon, J.R. and Hodgkins, W.R. (Eds), *Moving Boundary Problems in Heat Flow and Diffusion*, Clarendon Press, Oxford, p. 138.

Ouyang, T. and Tamma, K.K. (1996), "On adaptive time stepping approaches for thermal solidification processes", *Int. J. Numer. Methods for Heat and Fluid Flow*, Vol. 6 No. 2, pp. 37-50.

Rathjen, K.A. and Jiji, L.M. (1971), "Heat conduction with melting or freezing in a corner", *Journal of Heat Transfer, ASME*, Vol. 93, pp. 101-9.

Rubinsteĭn, L.I. (1971), "The Stefan problem", *Translations of Mathematical Monographs*, Vol. 27, American Mathematical Society, Providence, RI.

Sulfredge, C.D., Chow, L.C. and Tagavi, K.A. (1992), "Void formation in radial solidification of cylinders", *Journal of Solar Energy Engineering*, Vol. 114, pp. 32-9.

Voller, V. and Cross, M. (1981), "Accurate solutions of moving boundary problems using the enthalpy method", *Int. J. Heat and Mass Transfer*, Vol. 24, pp. 545-56.

Wang, X.Y. and Chang, S.C. (1999), "A 2D non-splitting unstructured triangular mesh Euler solver based on the space time conservation element and solution element method", *Computational Fluid Dynamics Journal*, Vol. 8 No. 2, pp. 309-25.

Wang, X.Y., Chang, S.C. and Jorgenson, P.C.E. (2000), "Prediction of sound waves propagating through a nozzle without/with a shock wave using the space-time CE/SE method", 38th AIAA Aerospace Sciences Meeting, Reno, NV, AIAA Paper 2000-0222.

Wang, X.Y., Chow, C.Y. and Chang, S.C. (1998), "The space-time conservation element and solution element method – a new high-resolution and genuinely multidimensional paradigm for solving conservation laws II. Numerical simulation of shock waves and contact discontinuities", NASA/TM-1998-208844.

Yang, D., Yu, S.T. and Zhao, J. (2001), "Convergence and error bound analysis for the space-time CESE method", *Numerical Methods for Partial Differential Equations*, Vol. 17, pp. 64-78.

Zhang, Z.C., Yu, S.T. and Chang, S.C. (2002), "A space-time conservation element and solution element method for solving the two- and three-dimensional unsteady Euler equations using quadrilateral and hexahedral meshes", *Journal of Computational Physics*, Vol. 175, pp. 168-99.